ACS OMEGA

Open Access

http://pubs.acs.org/journal/acsodf

Article

Hyaluronic Acid-Modified Luteolin−Copper Complex Nanodelivery System for Bacterial Prostatitis

Ruixiao Li,[#] Yunhe Zheng,[#] Xuelian Li, Ruiping Su, Jiangchuan He, Song Xue, Ke Wang,* Yanyao Gao,* and Jianxin Ni*

Cite This: *ACS Omega* 2024, 9, 42582−42592

Read Online

ACCESS | Metrics & More | Article Recommendations | Supporting Information

ABSTRACT: Bacterial prostatitis is a common disease of the male genitourinary system, which seriously affects the normal life and health of male patients. Antibiotics are commonly used in the clinical treatment of bacterial prostatitis, but the efficacy of fluoroquinolones is gradually declining due to the increasing drug resistance of bacteria. Hence, it is necessary to find new antibacterial drugs to treat bacterial prostatitis. Luteolin is a natural flavonoid compound with many pharmacological activities such as antibacterial and anti-inflammatory activities, but its poor water solubility and low structural stability seriously limit its clinical application. In this study, we designed a targeting drug delivery system via a luteolin−copper complex grafted with hyaluronic acid. The results of the characterization proved the successful synthesis of the system. The results of the in vitro performance test show that the system has a good antibacterial effect and excellent blood compatibility and can be effectively released under different pH conditions. The prepared nanodrug delivery system not only provides a new idea for the treatment of bacterial prostatitis but also lays a theoretical and practical foundation for the wide application of luteolin in clinical practice.

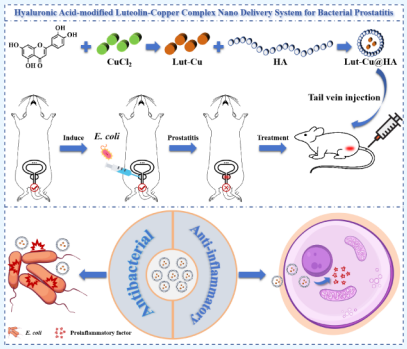

1. INTRODUCTION

Prostatitis is a prostate disease characterized by urinary tract irritation symptoms and chronic pelvic pain caused by various complex factors. Prostatitis is mainly classified into 4 types: (I) acute bacterial prostatitis (ABP), (II) chronic bacterial prostatitis, (III) chronic prostatitis/chronic pelvic pain syndrome, and (IV) asymptomatic inflammatory prostatitis.[1] Among them, acute bacterial prostatitis and chronic bacterial prostatitis are known as bacterial prostatitis. Bacterial prostatitis is one of the most common urogenital infections in males, with Gram-negative bacteria such as *E. coli* being the most common pathogen.[2] Fluoroquinolones are recommended as first-line antimicrobial agents for treating acute bacterial prostatitis. Unfortunately, the effectiveness of fluoroquinolones has gradually declined in recent years due to an increase in multiple resistant bacteria.[3] Therefore, there is a need to search for new drugs to treat bacterial prostatitis.

Luteolin (Lut) is a natural flavonoid widely distributed in nature that can be extracted from various plants, including those in the Araceae and Brassicaceae families. Luteolin not only serves as a natural pigment for dyeing but also acts as a medicinal active ingredient with diverse pharmacological activities, such as anti-inflammatory, antibacterial, antitumor, and antioxidant properties,[4] showing considerable potential for clinical applications. However, its tetracyclic flavonoid structure leads to poor ester affinity and high lattice energy due to the interactions between phenolic hydroxyl groups, resulting in low water solubility.[5] In addition, the phenolic hydroxyl groups are easily oxidized, reducing the structural stability of luteolin. These shortcomings result in low bioavailability, significantly limiting its widespread clinical use.

As a kind of natural flavonoid, luteolin can undergo coordination reactions with various metal ions, forming stable luteolin−metal complexes that enhance some pharmacological activities. Specifically, the antibacterial ability of luteolin is significantly improved upon coordination with copper ions.[6] Luteolin and copper ions coordinate to form luteolin−metal complexes, not only enhancing its structural stability and preventing oxidation-induced loss of activity but also significantly improving its antibacterial ability.[7] However, like most flavonoid−metal ion complexes, the water solubility of the luteolin−copper complex (Lut−Cu) remains poor, dissolving only in organic solvents such as dimethyl sulfoxide and pyridine, requiring further modification to improve water solubility.[8]

Hyaluronic acid (HA), a naturally macromolecular glycosaminoglycan, is composed of repeating disaccharide units of *N*-acetylglucosamine and D-glucuronic acid.[9] HA exists widely in living organisms and has an excellent biocompatibility. Its

Received: August 21, 2024
Revised: September 13, 2024
Accepted: September 18, 2024
Published: October 6, 2024

Scheme 1. Hyaluronic Acid-Modified Luteolin−Copper Complex Nanodelivery System for Bacterial Prostatitis

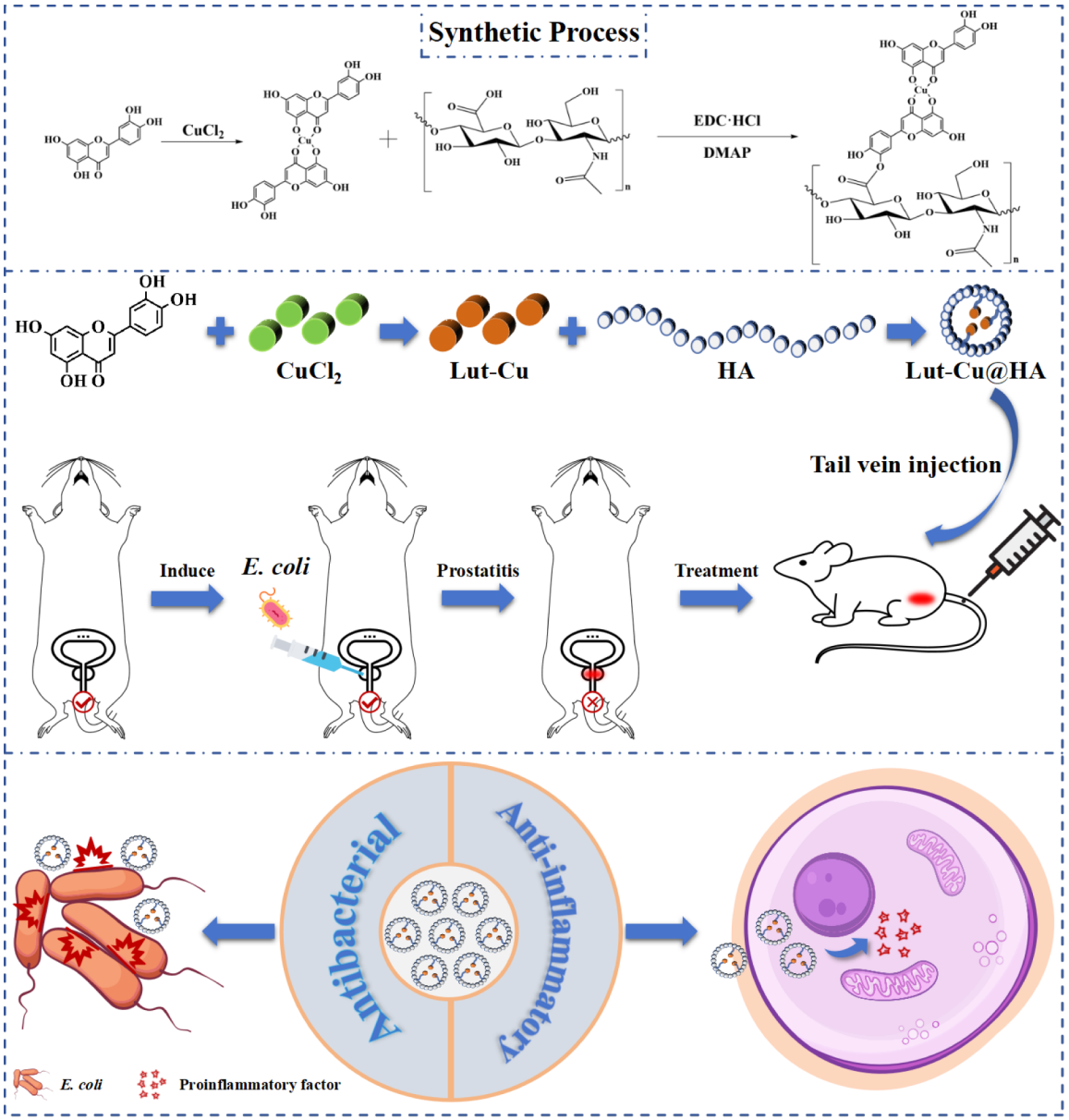

application spans cosmetics production and diverse ophthalmic surgical interventions such as corneal transplantation and lens implantation. Besides, HA exhibits significant clinical value in wound healing promotion and arthritis treatment.[10] Unlike other macromolecular glycosaminoglycans, HA avoids covalent protein binding, commonly existing as a free sodium salt with pronounced water solubility.[11] Studies indicate that the CD44 receptor exhibits increased expression at inflammatory sites and actively participates in the process of inflammation formation.[12] As a natural ligand for CD44, HA acts as a targeting molecule in drug delivery systems, effectively directing drugs to specific inflammatory sites.[10,12] At the same time, the carboxyl groups on the disaccharide unit of HA can be esterified with hydroxyl groups on the benzene ring of Lut or Lut−Cu. Lut−Cu and HA are connected by ester bonds, which enhance the water solubility of Lut−Cu and impart specific inflammatory targeting capabilities to the drug delivery system (Scheme 1). This leads to a significant enhancement in its bioavailability, better playing its anti-inflammatory, antibacterial, and other pharmacological effects.

In previous research, we developed a targeted drug delivery system of hyaluronic acid-modified curcumin−copper complex (Cur−Cu@HA), which showed some therapeutic effects in the treatment of bacterial prostatitis.[8] However, the bioavailability of curcumin is low. The highest plasma concentration of curcumin only reaches 0.05 μM,[13] whereas the highest plasma concentration of luteolin can reach 15 μM.[14] In LPS-stimulated macrophages, the inhibition by luteolin treatment on inflammatory gene expression is stronger than that by combined treatment with curcumin and PDTC,[15] indicating that luteolin has a more potent anti-inflammatory effect. Studies have shown that similar to gefitinib, luteolin can inhibit the growth of the metastatic prostate cancer cell line PC3,[16] suggesting that luteolin has greater potential in the treatment of prostate-related diseases. Additionally, luteolin has analgesic effects that can alleviate chronic inflammatory pain,[17] which curcumin does not have.

https://doi.org/10.1021/acsomega.4c07724
ACS Omega 2024, 9, 42582−42592

In summary, this study aims to construct a targeted drug delivery system of the hyaluronic acid-modified luteolin−copper complex (Lut−Cu@HA). The physical structure characterization will be performed using SEM, TEM, ^{1}H NMR, FT-IR, XPS, and XRD to confirm the successful synthesis of Lut−Cu@HA. Subsequent tests will include water solubility testing, in vitro drug release experiments, and antibacterial tests. Finally, the in vivo therapeutic efficacy was evaluated by establishing a rat model of bacterial infectious prostatitis. This not only provides a new idea for the treatment of bacterial prostatitis but also lays a theoretical and practical foundation for the extensive clinical application of luteolin.

2. MATERIALS AND METHODS

2.1. Materials. Luteolin (Lut, 98%) and anhydrous cupric chloride ($CuCl_2$, 98%) were obtained from Shanghai Macklin Biochemical Co., Ltd. Hyaluronic acid sodium salt (HA, Mw: 2.0×10^5 Da, PDI: 0.2, 98%) was purchased from Shanghai Yuanye Biological Technology. Hydrochloric acid, absolute ethyl alcohol, and dimethyl sulfoxide (DMSO, 99.7%) were obtained from Tianjin Fuyu Fine Chemicals Co., Ltd. 1-Ethyl-3-(3-dimethylaminopropyl) carbodiimide hydrochloride and 4-dimethylaminopyridine (EDC·HCl, 98.5%) were obtained from Shanghai Macklin Biochemical Co., Ltd. Sodium dodecyl benzene sulfonate (SDBS, 90%) was purchased from Tianjin Sciens Biochemical Technology Co., Ltd.

Male Sprague−Dawley (SD) (5−7 weeks old, 250 ± 30 g) rats were purchased from the Laboratory Animal Center of Xi'an Jiaotong University. They were fed at an animal facility of the IVC class (license no. SCXK (Shaanxi) 2015-002) with ad libitum access to food and water under controlled conditions (temperature of 20−22 °C, relative humidity of 50−60%, and 12-h day/night cycles). All animal experiments complied with the ARRIVE guidelines and were carried out in accordance with the U.K. Animals (Scientific Procedures) Act, 1986.

2.2. Synthesis of the Luteolin−Copper Complex. The coordination of luteolin with metal ions increases its structural stability considerably and enhances some of its physiological activities. Lut−Cu was synthesized as follows[8,18]: 0.1431 g of luteolin was precisely weighed in a 100 mL flask and 20 mL of anhydrous ethanol was added. The flask was magnetically stirred at 50 °C on a magnetic stirrer equipped with a reflux condenser to fully dissolve luteolin. Then, 5 mL of the prepared 0.05 mol/L $CuCl_2$ solution was added dropwise to the completely dissolved luteolin solution using a pasteurized dropper. After the reaction system cooled to room temperature, the pH of the system was adjusted to around 8 using a suitable amount of 1 mol/L NaOH solution (≈2 mL). Next, 5 mL of the prepared 0.025 mol/L SDBS solution was added. The reaction system was then stirred at 60 °C on a magnetic stirrer equipped with a reflux condenser for 8 h. After cooling to room temperature, the reaction system was filtered, and the precipitate was washed with deionized water and anhydrous ethanol 3 times. The precipitate on the filter paper was placed in a vacuum drying oven at 50 °C to dry, resulting in a brownish-yellow solid of Lut−Cu. The complex was stored in the dark at 4 °C for later use.

2.3. Preparation and Characterizations of Lut−Cu@HA Nanoparticles. *2.3.1. Preparation of Lut−Cu@HA Nanoparticles.* The disaccharide units constituting hyaluronic acid feature carboxyl groups, which can undergo esterification reactions with hydroxyl groups on the phenyl ring of Lut or Lut−Cu. Lut-Cu@HA was synthesized as follows:[8,19] 200 mg of HA was weighed in a 250 mL flask, and 40 mL of the prepared 50% DMSO aqueous solution was added. The flask was magnetically stirred at 60 °C on a magnetic stirrer equipped with a reflux condenser to fully dissolve the HA. To activate the carboxyl groups in HA, a suitable amount of EDC·HCl and DMAP was added into the completely dissolved HA solution. After 1 h of activation, 50 mL of a DMSO solution containing 65.2 mg of Lut-Cu was added. Following 6 h of stirring the reaction system, the reaction solution was transferred to a preactivated dialysis bag and it was dialyzed in deionized water for 3 d. Upon completion of dialysis, the precipitate was removed through filtration, and the solution was subjected to freeze-drying to obtain Lut−Cu@HA. The product is a brownish-yellow flocculent solid and should be stored in the dark at 4 °C for later use.

2.3.2. Characterizations of Lut−Cu@HA Nanoparticles. The Fourier-transform infrared spectra (FT-IR) of Lut, Lut−Cu, HA powders, and lyophilized Lut−Cu@HA samples were analyzed in the range of 400 to 4000 cm^{-1} using an FT-IR spectrometer (Nicolet iS 50, Thermo Fisher). Besides, the chemical structure of Lut−Cu@HA nanoparticles was analyzed through ^{1}H NMR analysis conducted on a 400 MHz nuclear magnetic resonance (NMR) spectrometer (JNM-ECZ 400 S/L1, JEOL, Japan) at room temperature. Deuterium oxide (D_2O) served as the solvent with tetramethylsilane (TMS) employed as the reference compound. The elemental composition, encompassing the full spectrum and narrow spectrum of Cu in Lut−Cu and Lut−Cu@HA samples, was ascertained using an X-ray photoelectron spectrometer (ESCALAB Xi+, Thermo Fisher, USA) following established protocols. Lut−Cu, Lut-Cu@HA, Lut, and HA powders underwent scanning in the range of 5−80° using an X-ray diffractometer (XRD 6100, Japan). Finally, particle size, polydispersity index (PDI), and zeta potential values were determined using a nanoparticle size and a zeta potential analyzer (ZSE, Malvern, UK). Morphological characteristics and elemental distribution were observed through scanning electron microscopy (SEM) and transmission electron microscopy (TEM).[20]

2.3.3. Water Solubility Improvement of Lut−Cu@HA Nanoparticles. 10 mg of Lut, Lut−Cu, and Lut−Cu@HA were weighed into three identical glass bottles. 15 mL of deionized water was added to each bottle and shaken well after ultrasonic shock for even dispersion. The state of the solution in each bottle was observed. After they were allowed to stand for 3 h, the state of the solution in each bottle was observed again and compared with their initial states. Excess amounts of Lut−Cu and Lut−Cu@HA were weighed and prepared as saturated solutions in 5 mL of deionized water. The mixtures were then swirled on a whirlpool mixer for 3 min, followed by ultrasonic shock for 20 min to ensure complete dissolution. Subsequently, centrifugation was performed at a rotating speed of 15 000 rpm for 8 min. Finally, the supernatant was collected to determine the absorbance value of each solution at the maximum absorption wavelength of Lut−Cu. These values were compared to those of a pure Lut−Cu aqueous solution and the Lut−Cu content was calculated in each solution according to the Beer−Lambert law.[21]

2.3.4. In Vitro Antibacterial Activity Evaluation. The removal of pathogens is key to the treatment of bacterial prostatitis, with *E. coli* being a common cause. To evaluate the ability of Lut−Cu@HA to eliminate *E. coli*, we used the plate counting method to test its antibacterial performance.[22] In

https://doi.org/10.1021/acsomega.4c07724
ACS Omega 2024, 9, 42582−42592

brief, 1 mL of bacterial suspension (1×10^4 CFU/mL) was added to a shaking tube and incubated at 37 °C for 1 h. Subsequently, 20 μL of the bacterial suspension (diluted in PBS) was cultured overnight at 37 °C on a plate counting agar (PCA). The antibacterial activity of Lut, Lut−Cu, and Lut−Cu@HA was determined using PBS as the blank control. Each group was tested 3 times, and the colony-forming units (CFUs) were counted. The antibacterial rate was calculated using the following equation:

$$\text{antibacterial rate (\%)} = \frac{\text{CFU of control group} - \text{CFU of experimental group}}{\text{CFU of control group}} \times 100\%$$

2.3.5. In Vitro Release of Lut−Cu. To determine the drug release characteristics in blood and at inflammatory sites, two portions of Lut−Cu@HA weighing 10.0 mg each were precisely measured and dissolved in 5 mL of the prepared PBS buffer solutions (pH 5.0 and pH 7.4) separately. The solution was then loaded into preactivated dialysis bags (8000−14 000 Da) and securely sealed at both ends with lines. The dialysis bag was placed in 50 mL of release media corresponding to pH, and the entire system was placed in a 37 °C constant temperature water bath shaker for continuous agitation. At various time points, 2 mL of the release media was withdrawn by a pipet and diluted by half with the release media corresponding to pH. The absorbance (OD) values were measured at 350 nm using a UV−visible spectrophotometer. During the drug release process, the PBS buffer solution corresponding to pH was supplemented to maintain the release media volume at 50 mL. The release rate was calculated using the following equation:[23]

$$\text{antibacterial rate (\%)} = \frac{\text{the total quantity of drug} - \text{the released quantity of drug}}{\text{the total quantity of drug}} \times 100\%$$

2.3.6. In Vitro Biocompatibility Assay of Lut−Cu@HA. Biocompatibility is one of the important indicators for evaluating drugs. To evaluate the in vitro biocompatibility of Lut−Cu@HA, RAW 264.7 and L929 cells were used in MTT assays.[24] In brief, cells were seeded in a 96-well plate at a density of 2×10^4 cells/well (200 μL/well). After the cells were incubated in a cell culture incubator for 24 h, various concentrations of sterilized Lut−Cu@HA (50, 100, 200, 400, or 800 μg) were added to the wells. After an additional 24 h, the culture medium was removed by a pipet, and 200 μL of MTT solution (5 mg/mL) was added to each well in the dark. The plate was then incubated at 37 °C for 6−8 h. After MTT incubation, the solution was removed, and 150 μL of DMSO was added to each well. The plate was shaken on a shaker for 15 min to fully dissolve formazan. The OD values at 490 nm were measured by using a microplate reader. The cell viability was calculated using the following equation:

$$\text{cell viability (\%)} = \frac{\text{experimental OD} - \text{blank OD}}{\text{negative control OD} - \text{blank OD}} \times 100\%$$

2.4. Antibacterial Prostatitis Effect In Vivo by Lut−Cu@HA Nanoparticles. A bacterial prostatitis model was established by referencing the methodology outlined in previous studies.[8,25] In brief, male SD rats were anesthetized and a 1.5 cm incision was made in the lower abdomen. The bladder was carefully pulled out from the abdominal cavity to fully expose the bladder, seminal vesicles, and prostate. 50 μL of the prepared *E. coli* bacterial suspension (1×10^8 CFU/mL) was injected into each lobe of the prostate using an insulin needle. The bladder was then gently pushed back into the abdominal cavity using a sterile cotton swab. The muscle tissue and skin were sutured layer by layer. After suturing, a small amount of penicillin was injected subcutaneously around the incision, followed by disinfection with iodine. The entire surgery was conducted under sterile conditions.

For treatment, levofloxacin (LEVO), a commonly used fluoroquinolone in the clinical treatment of bacterial prostatitis, was chosen as the positive control. The rats were divided into five groups: normal group, model group, LEVO group, low dose group, and high dose group. On day 0, rats in the model group, the LEVO group, the low dose group, and the high dose group received an intraprostatic injection of a certain amount of *E. coli* bacterial suspension, while the rats in the normal group received an equivalent amount of saline. The LEVO group received levofloxacin at a dose of 40 mg/kg, while the low dose and the high dose groups received Lut-Cu@HA nanoparticles at doses of 10 and 30 mg/kg. The drugs were injected via tail vein on days 1, 3, and 5. On day 7, rats were euthanized with carbon dioxide (CO_2), and prostate tissues and relevant immune organs were collected to evaluate the therapeutic effects.

2.5. Body Weight Change and Organ Index. The weight of each rat was recorded daily to analyze the trends in their weight changes. On day 7, rats were euthanized with CO_2, and prostate tissues and relevant immune organs were weighed. The organ index was calculated using the following equation:[26]

$$\text{organ index} = \frac{\text{tissue weight}}{\text{body weight}} \times 10\,000$$

2.6. Histopathological Examination. To evaluate the therapeutic effects of Lut−Cu@HA on bacterial prostatitis, tissues from each group of rats were subjected to hematoxylin and eosin (H&E) staining and Masson staining.[27] In brief, the collected tissues were promptly fixed in a 4% paraformaldehyde solution, embedded in paraffin, and sectioned into tissue slices (5 μm). The slices were stained with H&E or Masson reagents, and the staining results were observed using a slide scanner.

2.7. Immunofluorescent Staining. To further study the inflammatory process, double immunofluorescence staining was conducted on prostate tissues from each group of rats.[28] In brief, tissue sections (5 μm) underwent deparaffinization and rehydration, followed by blocking with goat serum to prevent nonspecific antibody binding. Subsequently, incubation with primary and secondary antibodies occurred, and the secondary antibodies were labeled by using Alexa Fluor 594 and Alexa Fluor 488. Finally, staining with 4′,6-diamidino-2-phenylindole (DAPI) took place at room temperature for 10 min. The immunofluorescent staining results were observed using a fluorescence microscope (NIKON ECLIPSE TI-SR, Japan).

2.8. In Vivo Biocompatibility and Organ Toxicity Study. To evaluate the in vivo biocompatibility and organ toxicity of Lut−Cu@HA nanoparticles, hemolysis tests and rat intravenous injection experiments were conducted. The hemolysis ratio of Lut−Cu@HA was determined using the red blood cell suspensions of rats.[29] In brief, various concentrations of Lut−Cu@HA were added to 1 mL of 2%

https://doi.org/10.1021/acsomega.4c07724
ACS Omega 2024, 9, 42582−42592

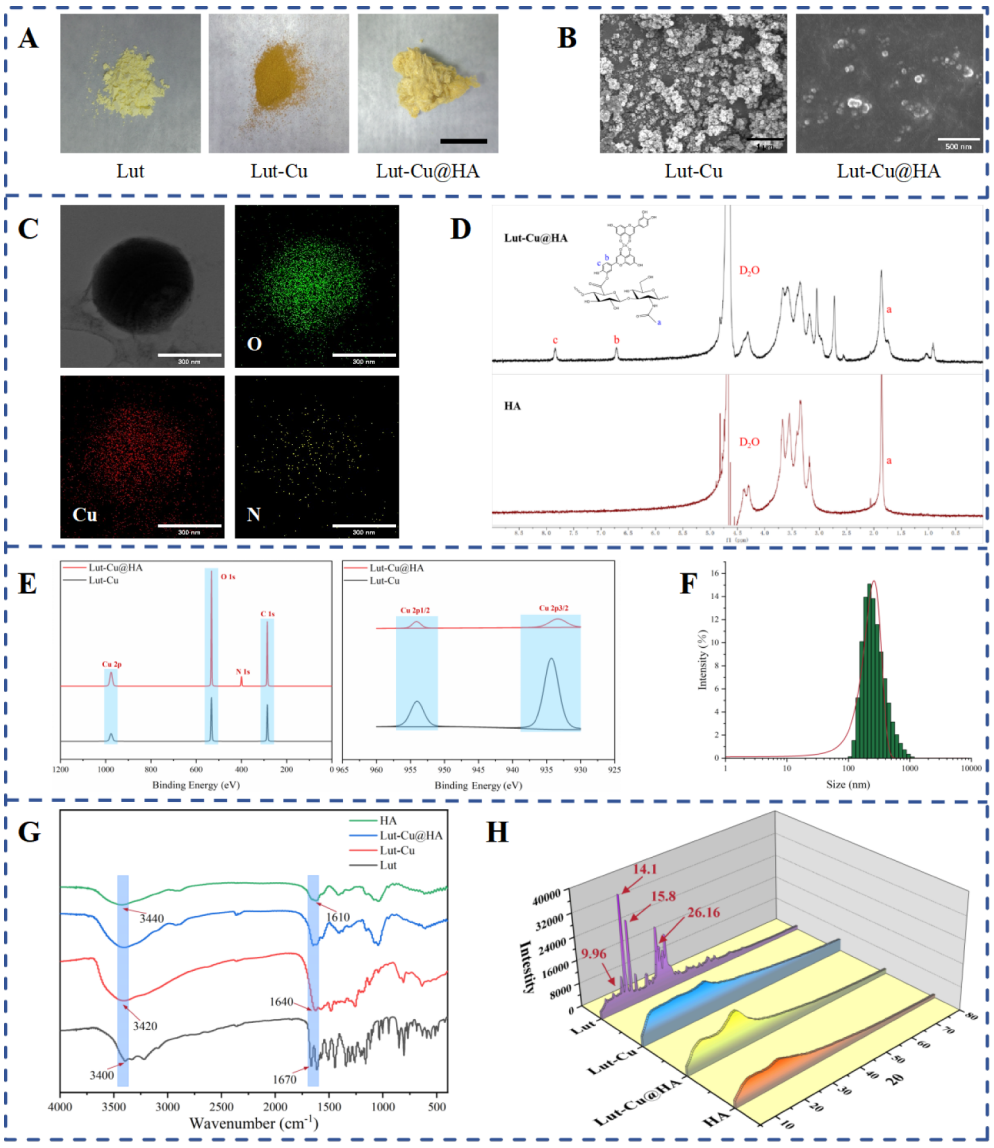

Figure 1. Characterizations of Lut−Cu@HA nanoparticles. (A) The photos of Lut, Lut−Cu, and Lut−Cu@HA; scale bar = 2 cm. (B) The SEM images of Lut−Cu solid and Lut−Cu@HA solution. (C) The TEM and EDS images of Lut−Cu@HA. (D) The ^{1}H NMR spectra of Lut−Cu@HA and HA. (E) The XPS images of Lut−Cu and Lut−Cu@HA. (F) The grain size profile of Lut−Cu@HA. (G) The FT-IR graphs of HA, Lut, Lut−Cu, and Lut−Cu@HA. (H) The XRD patterns of HA, Lut, Lut−Cu, and Lut−Cu@HA.

human red blood cell suspension, which was diluted with normal saline (NS), and then incubated at 37 °C for 3 h. NS served as the negative control, and a 1% Triton X-100 aqueous solution served as the positive control. Subsequently, the suspensions were centrifuged at 1500 rpm for 10 min. After centrifugation, the OD values of the supernatant were measured at 545 nm. The hemolysis ratio was calculated using the following equation:

$$\text{hemolysis ratio} = \frac{\text{experimental OD} - \text{negative control OD}}{\text{positive control OD} - \text{negative control OD}} \times 100\%$$

In addition, a specific volume of Lut−Cu@HA solution and an equivalent volume of NS were injected via the tail vein into two groups of rats. On day 7, rats were euthanized with CO_2. Major organs such as the heart, liver, spleen, lung, and kidney were collected for H&E and Masson staining, conducting histopathological evaluations, and analyzing the organ toxicity.[30]

2.9. Statistical Analysis. All data were presented as mean ± standard deviation (SD). Statistical significance was assessed by one-way analysis of variance (ANOVA) conducted with GraphPad Prism 9.0.0 (GraphPad, San Diego, CA). A significance level of $p < 0.05$ was considered indicative of statistically significant differences.

3. RESULTS AND DISCUSSION

3.1. Preparation and Characterizations of Lut−Cu@HA Nanoparticles. After the synthesis of Lut−Cu@HA, the morphologic characteristics were observed via a digital camera. As shown in Figure 1A, Lut and Lut−Cu were powdery solids, and after coordination with copper ions, the color of Lut deepened from light yellow to brownish-yellow. After freeze-drying Lut−Cu@HA, a yellow flocculent material formed, conforming to the freeze-dried morphology of macromolecular polysaccharides. Subsequently, the microstructure was observed by SEM (Figure 1B). Lut−Cu powder showed a cluster-

https://doi.org/10.1021/acsomega.4c07724
ACS Omega 2024, 9, 42582−42592

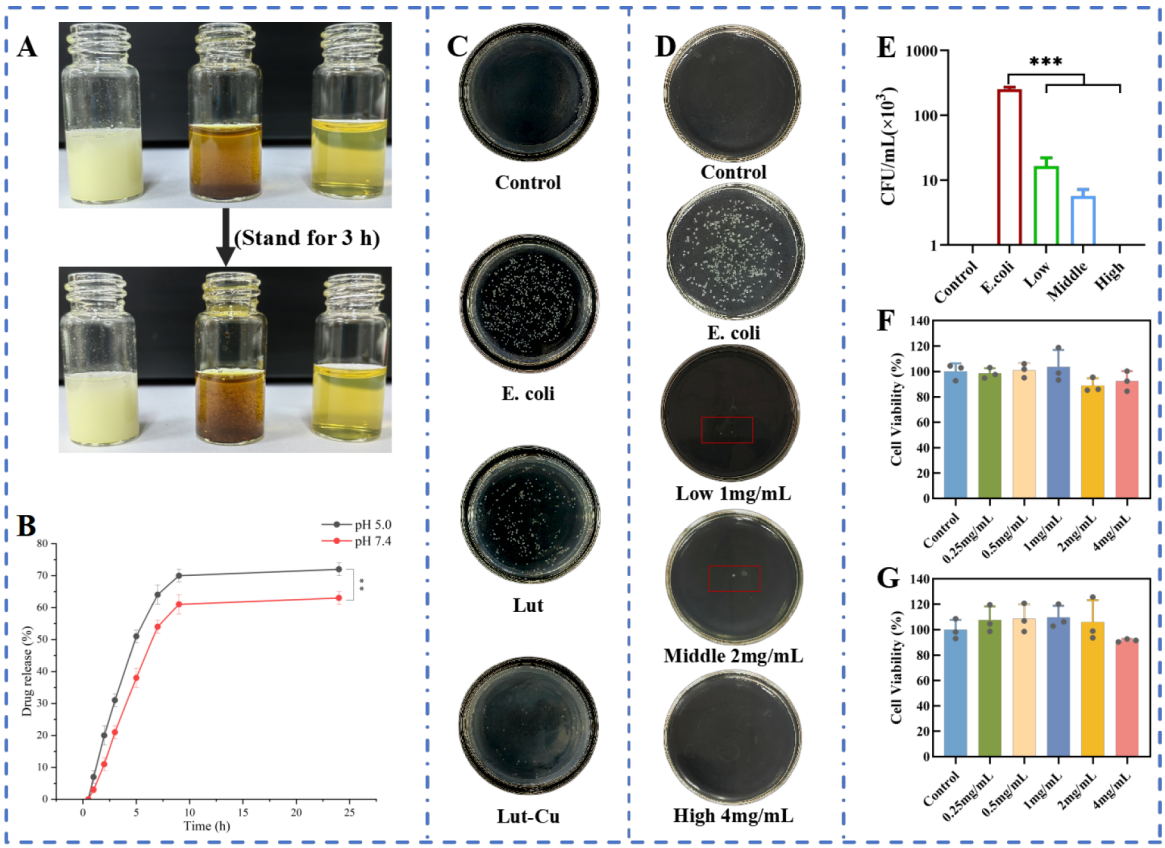

Figure 2. In vitro performance testing of Lut−Cu@HA nanoparticles. (A) The water solubility of Lut, Lut−Cu, and Lut−Cu@HA. (B) The in vitro release results under acidic and neutral conditions. (C) The antibacterial ability test of Lut and Lut−Cu. (D) The antibacterial ability test of Lut−Cu@HA. (E) The statistical result of CFU of panel D. (F) The cell viability results of L929. (G) The cell viability results of RAW264.7. Data are mean ± SD, $n = 3$; ***$p < 0.005$.

like particle morphology, which may be due to water loss and aggregation during the vacuum drying process. Lut−Cu@HA spherical nanoparticles were formed in an aqueous solution due to their amphiphilic nature. The molecule possesses both the hydrophilicity of HA and the hydrophobicity of Lut−Cu. This amphiphilic structure allows the macromolecule to self-assemble into spherical nanoparticles in an aqueous solution. Finally, the internal structure was observed by TEM, and the elemental distribution was analyzed via energy-dispersive X-ray spectroscopy (EDS) (Figure 1C). The obvious enrichment of Cu, N, and O was observed in the spherical nanoparticle regions, with the Cu element content being approximately 24%, confirming the successful synthesis of Lut−Cu@HA. Additionally, the structures of Lut−Cu and Lut−Cu@HA were further confirmed by XPS. As shown in Figure 1E, the N element was detected in Lut−Cu@HA but not in Lut−Cu, further confirming the successful binding between Lut−Cu and HA. The Cu element was detected in both Lut−Cu and Lut−Cu@HA, indicating the successful coordination of Lut with Cu. The average particle size of Lut−Cu@HA was around 380 nm (Figure 1F), which is slightly smaller than that of Cur−Cu@HA,[8] exhibiting a small and uniformly distributed size consistent with the observation results from TEM. The particle size of Lut−Cu grafted with HA increased, suggesting the encapsulation effect of HA on Lut−Cu. The PDI of Lut−Cu@HA was around 0.25, fewer than 0.3, further confirming the uniform size distribution of the nanoparticles. Additionally, the zeta potential values were consistently around −32 mV, indicating the stability of the Lut−Cu@HA nanoparticles. ^{1}H NMR spectrum showed obvious $-CH_3$ hydrogen signals at 1.86 (peak a) for HA, originating from the methyl group of its disaccharide unit (Figure 1D). After the esterification reaction between Lut−Cu and HA to form Lut−Cu@HA, new hydrogen signals appeared at 6.72 and 7.84 (peaks b and c) due to the benzene ring of Lut−Cu. Compared to pure HA, benzene ring hydrogen signals were observed in the ^{1}H NMR spectrum of Lut−Cu@HA, further confirming the successful grafting of Lut−Cu onto HA.

In the FT-IR graph (Figure 1G), the stretching vibration absorption peaks for phenolic hydroxyl groups (O−H) at 3400 cm^{-1} and carbonyl groups (C═O) at 1670 cm^{-1} appeared in Lut. After coordination with copper ions to form Lut−Cu, changes were observed in the absorption peaks of the phenolic hydroxyl groups and carbonyl groups. Specifically, the carbonyl group (C═O) stretching vibration absorption peak in Lut−Cu shifted from 1670 to 1640 cm^{-1}, indicating the weakening of the C═O bond due to coordination with O in the C-ring of Lut. Compared with Lut, the stretching vibration absorption peak of hydroxyl groups (O−H) in Lut−Cu shifted from 3400 to 3420 cm^{-1} due to coordination with the hydroxyl group of C5 in the A-ring.[31] The broad peaks at 3440 and 1610 cm^{-1} appeared in HA, corresponding to the stretching vibrations of hydroxyl (O−H) and carboxyl groups (C═O), respectively. After the esterification reaction to form Lut-Cu@HA, only minimal changes were observed in the absorption peaks of the phenolic hydroxyl and carboxyl groups, which may be due to the low drug loading and limited ester bond formation. XRD patterns showed that complex multipeak patterns within the

https://doi.org/10.1021/acsomega.4c07724
ACS Omega 2024, 9, 42582−42592

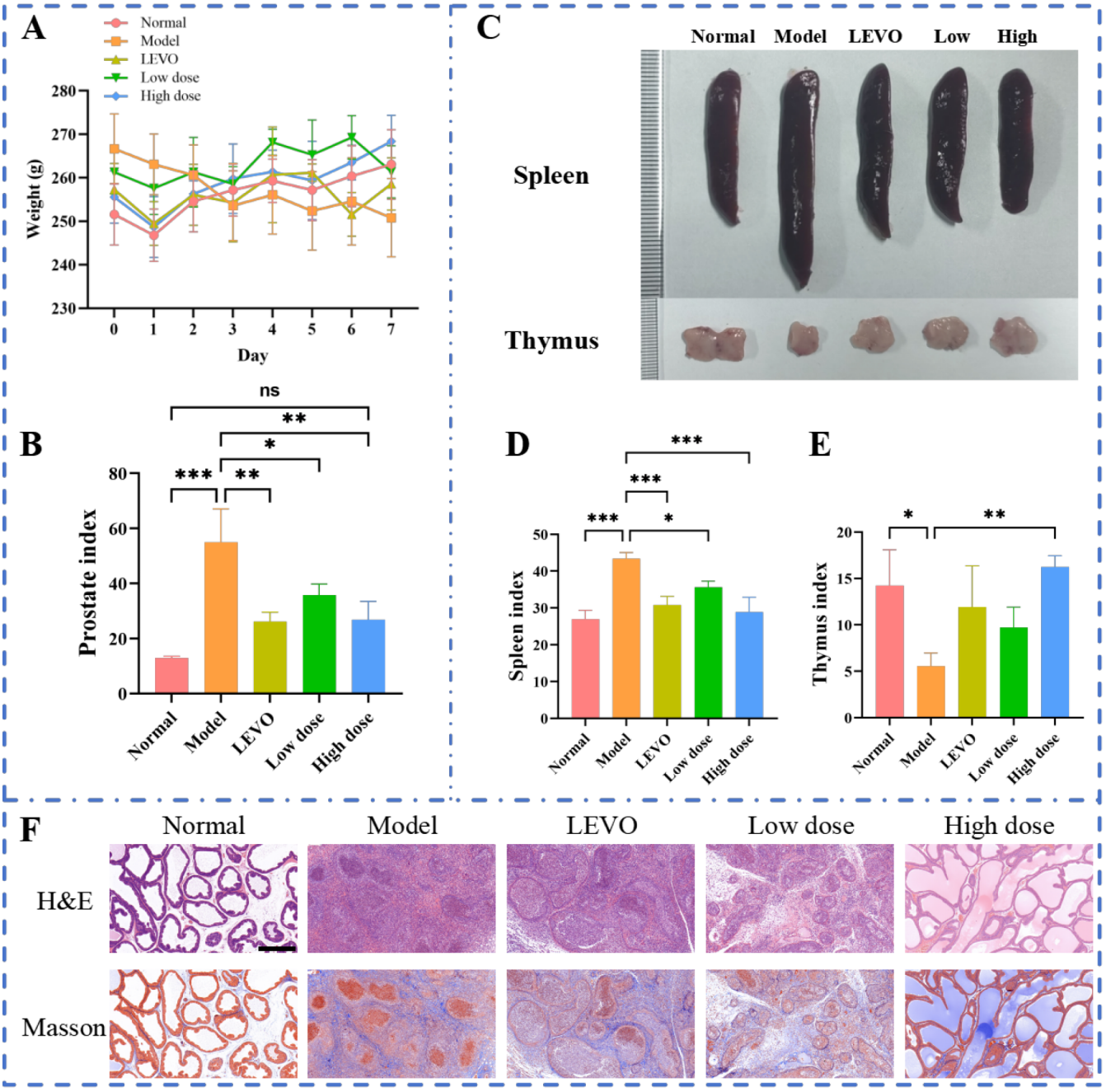

Figure 3. Therapeutic effect of Lut−Cu@HA for bacterial prostatitis in rats. (A) The body weight change curves in different groups. (B) The statistical results of the prostate index in different groups. (C) The photos of spleen and thymus in different groups. (D) The statistical results of the spleen index in different groups. (E) The statistical results of the thymus index in different groups. (F) The H&E staining and Masson staining results of prostate tissue in different groups. Data are mean ± SD, $n = 3$; *$p < 0.05$, **$p < 0.01$, ***$p < 0.005$. Scale bar = 500 μm.

range of 10° to 40° were observed in Lut (Figure 1H), indicating a highly crystalline structure.[32] Among them, characteristic peaks at 9.96°, 14.1°, 15.8°, and 26.16° were observed in Lut. However, relatively smooth peak shapes in the range of 10° to 40° were observed in Lut−Cu and Lut−Cu@HA, suggesting a transition from a highly crystalline state to an amorphous state after the coordination of Lut with copper ions.[33]

3.2. Water Solubility Improvement Experiment. The poor water solubility of Lut limited its widespread clinical application. To solve this problem, we grafted Lut onto HA to improve its water solubility. As shown in Figure 2A, after mixing equal masses of Lut, Lut−Cu, and Lut−Cu@HA with deionized water, Lut and Lut−Cu were suspended in water with visible particles suspended in the water. In contrast, Lut−Cu@HA fully dissolved in water, resulting in a clear and transparent solution without visible insoluble substances. After standing for 3 h, some particles of Lut and Lut−Cu gradually settled to the bottom of the glass bottle, maintaining the overall turbid suspension state. In contrast, the Lut−Cu@HA aqueous solution remained clear and transparent, indicating a significant improvement in the water solubility of Lut−Cu after modification with HA. Lut has a maximum absorption at 350 nm, and a standard curve was established by linear regression

https://doi.org/10.1021/acsomega.4c07724
ACS Omega 2024, 9, 42582−42592

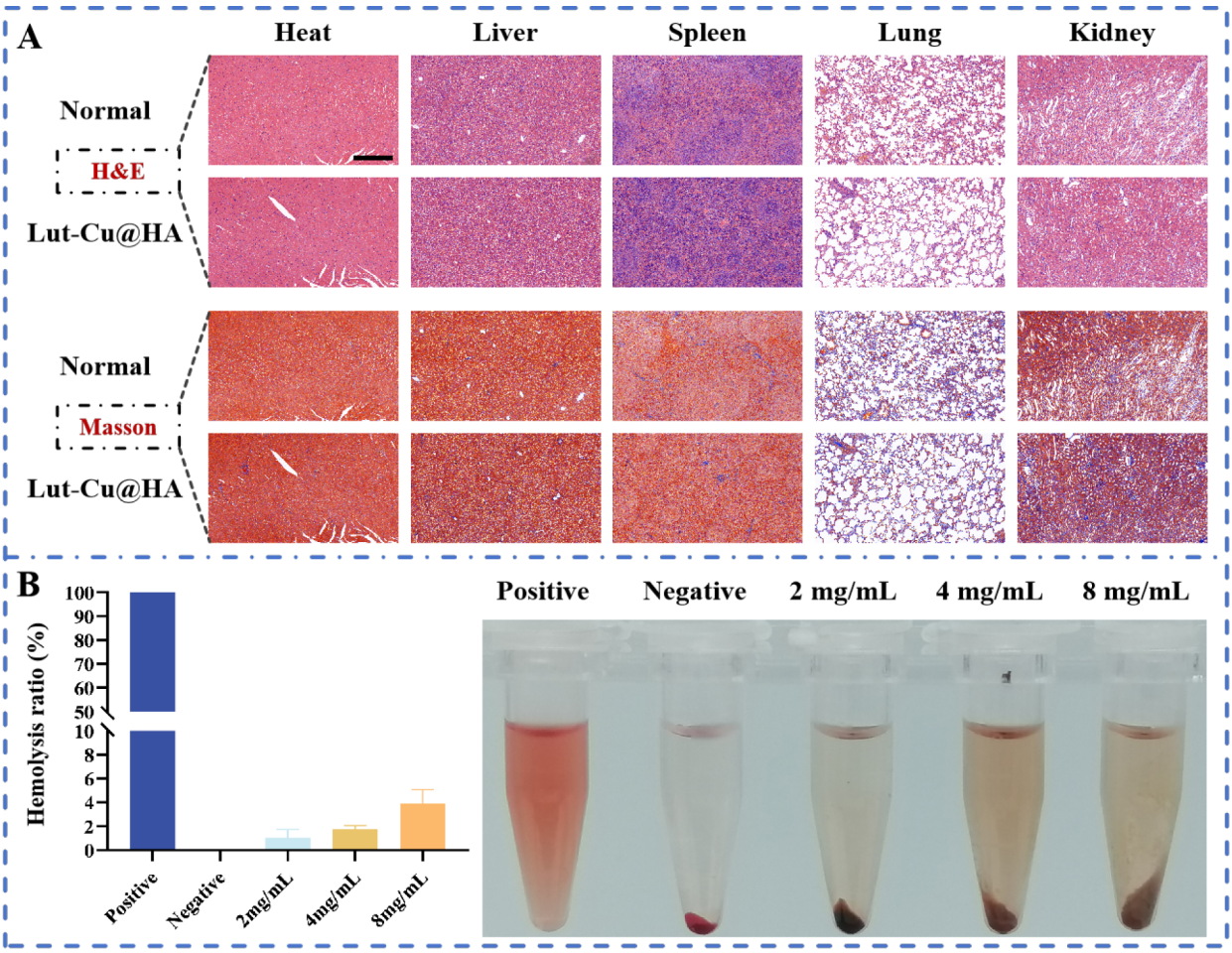

Figure 4. Biocompatibility of Lut−Cu@HA nanoparticles. (A) The H&E staining and Masson staining results of the heart, liver, spleen, lung, and kidney tissue. (B) The hemolysis ratio of Lut−Cu@HA. Scale bar = 500 μm.

(Figure S1). The OD value of the saturated Lut−Cu solution at 350 nm was measured as 0.082, and the corresponding concentration of the saturated Lut−Cu solution was calculated to be 4.8 μg/mL by the regression equation. While the OD value of a 10-fold-diluted saturated Lut−Cu@HA solution reached 0.223, the corresponding concentration of saturated Lut−Cu@HA solution was about 155 μg/mL. Thus, it is evident that the water solubility of Lut−Cu is improved by about 32 times after modification with HA.

3.3. In Vitro Release Test. During inflammation, the pH of the local microenvironment decreases to weak acidity,[34] and prostatitis is no exception. Therefore, acid-mediated rapid drug release can improve the therapeutic effectiveness of prostatitis. As shown in Figure 2B, Lut−Cu@HA demonstrated a drug release rate (Lut−Cu) of 60% within 24 h in PBS buffer solutions at pH ≈ 7.4 and pH ≈ 5.0. Interestingly, the drug release was faster in the PBS buffer solution at pH ≈ 5.0. This is because the acidic conditions expedite the cleavage of ester bonds in Lut−Cu@HA, leading to a quicker release of Lut−Cu. Given that the pH in the blood is neutral, while the pH in the inflammatory site is acidic, Lut−Cu@HA exhibits better drug release in the microenvironment of the inflammatory site, aligning with expectations.

3.4. Antibacterial Ability Test. To verify the enhanced antibacterial capability of Lut through copper ion coordination, antibacterial tests were conducted for both Lut and Lut−Cu. As shown in Figure 2C, Lut exhibited poor inhibition against *E. coli*, possibly due to its poor water solubility, hindering its antibacterial efficacy. In contrast, after coordinating with copper ions to form Lut−Cu, a significant reduction in *E. coli* colonies was observed, suggesting that Lut−Cu gradually releases copper ions in the solution, thereby enhancing its antibacterial effect. From the culture medium, it can be observed that the antibacterial effect of Lut−Cu is significantly stronger than that of Lut, while there is no significant difference in the antibacterial effect between Cur−Cu and Cur.[8] This indicated that Lut−Cu possessed a stronger antibacterial performance.

To further verify the antibacterial capability of the drug delivery system, antibacterial tests were conducted on Lut−Cu@HA at different concentrations. As shown in Figure 2D, Lut−Cu@HA exhibited significant inhibition against *E. coli*. With the increase in concentration, the number of bacterial colonies on the culture medium gradually decreased (Figure 2E), showing an obvious concentration dependence.

3.5. In Vitro Biocompatibility Assay. Qualified drugs must possess an excellent biocompatibility. As shown in Figure 2F,G, the cell viability of L929 and RAW 264.7 cells remained above 90% in different concentrations of Lut−Cu@HA solution. These results showed that when in contact with cells, Lut−Cu@HA nanoparticles did not induce toxicity or adverse effects on cells. This illustrated the good biocompatibility of the Lut−Cu@HA nanoparticles.

https://doi.org/10.1021/acsomega.4c07724
ACS Omega 2024, 9, 42582−42592

3.6. Efficacy Evaluation of Lut−Cu@HA against Bacterial Prostatitis in Rats. Previously, we conducted comprehensive in vitro tests of the Lut−Cu@HA nanodrug delivery system. The results showed that Lut−Cu@HA exhibited excellent water solubility, outstanding antibacterial ability, remarkable in vitro release performance, and good biocompatibility. These findings suggest that Lut−Cu@HA has significant potential in treating bacterial prostatitis. To further study its therapeutic effects, we established a rat model of bacterial prostatitis induced by *E. coli*. The rats were grouped and treated via tail vein injection to evaluate the efficacy of Lut−Cu@HA in treating bacterial prostatitis and to explore its potential application in the treatment of bacterial prostatitis. As shown in Figure 3A, there was no significant difference in the body weight change of the treated rats compared to the normal group, and no death of rats was observed during the experiment, proving that the selected dosage did not have obvious toxic side effects. Compared with the normal group, rats in the model group exhibited enlarged and hardened prostates, confirming the successful construction of the model. The prostate size of rats in the LEVO group, the low dose, and the high dose group was smaller than that in the model group (Figure 3B), indicating an improvement in bacterial prostatitis in the treated rats. Compared with the normal group, rats in the model group showed enlarged spleens and atrophied thymuses (Figure 3C−E), indicating inflammatory responses. However, the sizes of spleens in the LEVO group, the low dose, and the high dose groups were smaller than those in the model group, and thymuses were larger, indicating a partial recovery from bacterial prostatitis in the treated rats. These observations further validated the potential of the Lut−Cu@HA nanodrug delivery system in treating bacterial prostatitis.

3.7. Histopathological Examination. After collecting the prostates from each group of rats, histopathological examination was conducted through H&E staining and Masson staining. As shown in Figure 3F, compared to the normal group, the prostates of rats in the model group exhibited inflammatory cell infiltration in the stroma, glands, and surrounding tissues, accompanied by tissue damage and lymph nodules. However, the prostates of the treated rats showed a significant reduction in inflammatory cell infiltration, especially in the high dose group, indicating the remarkable therapeutic effect of high-dose Lut−Cu@HA on bacterial prostatitis.

3.8. Biocompatibility of Lut−Cu@HA Nanoparticles. Previously, we conducted in vitro biocompatibility tests on Lut−Cu@HA nanoparticles, and the results showed that they have excellent cellular compatibility. To further evaluate the in vivo biocompatibility of Lut−Cu@HA nanoparticles, we conducted in vivo biocompatibility tests. One week after intravenous injection, the major organs of rats were collected, and then we performed histopathological analysis by H&E staining and Masson staining. As shown in Figure 4A, there was no obvious difference between the normal group and the Lut−Cu@HA group. The phenotype of cardiomyocytes was normal with a regular arrangement and no signs of inflammation. Similarly, no pathological abnormalities were observed in the hepatic sinusoids. The spleen tissue exhibited a normal white and red pulp. The lung tissue showed no alveolar expansion or collapse, and there were no signs of inflammatory cell proliferation or edematous changes. In addition, the renal tubules and glomeruli in the Lut−Cu@HA group displayed health similar to that of normal kidney tissue. These results emphasized that Lut−Cu@HA had no obvious organ toxicity in vivo. In the hemolysis tests, no blood toxicity was observed in the Lut−Cu@HA group. Compared to the negative control, the hemolysis in the Lut−Cu@HA group was negligible (Figure 4B), further demonstrating its safety for intravenous injection. Overall, these results further confirm the outstanding biocompatibility of Lut−Cu@HA, providing strong support for its significant potential in treating bacterial prostatitis.

3.9. Immunofluorescent Staining. It is well-known that TNF-α is a crucial proinflammatory factor capable of promoting inflammatory responses and inducing other cells to produce inflammatory factors. At the same time, NF-κB is activated under inflammatory conditions, further promoting the expression of the inflammatory factors. TNF-α can activate the NF-κB signaling pathway, causing NF-κB to enter the nucleus and stimulate the expression of inflammatory factors.[35] In this study, we utilized double immunofluorescence staining to assess the expression levels. The model group exhibited significant red fluorescence (NF-κB) and green fluorescence (TNF-α) (Figure 5A), indicating a significant inflammatory response in the model group. In contrast, in the high dose group, we observed a small amount of red fluorescence, with green fluorescence nearly imperceptible. Overall, these results indicated a significant anti-inflammatory effect of Lut−Cu@HA.

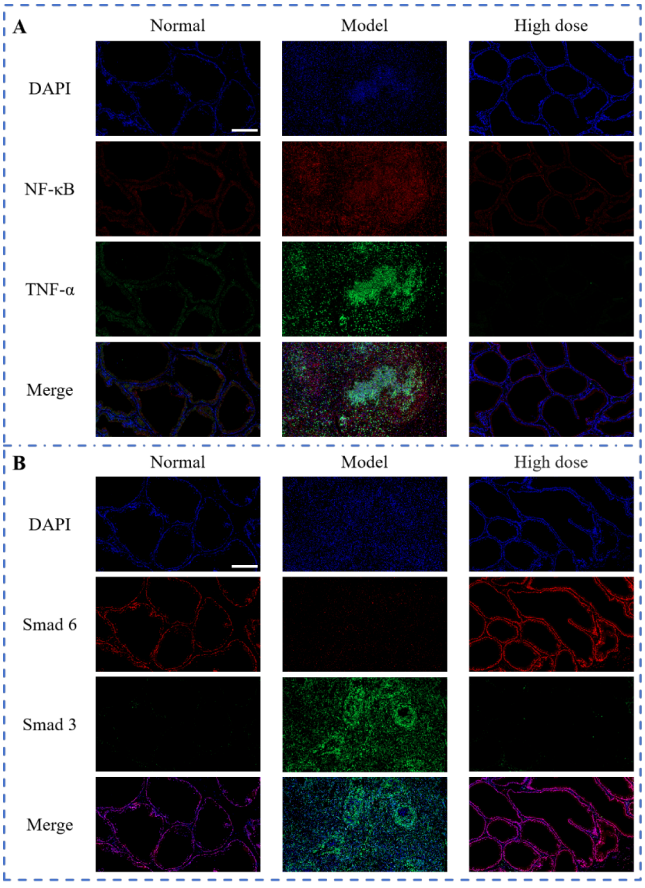

Figure 5. Representative immunofluorescence staining of different groups. (A) The sections of tissue stained with DAPI (blue), NF-κB (red), and TNF-α (green). (B) The sections of tissue stained with DAPI (blue), Smad 6 (red), and Smad 3 (green). Scale bar: 200 μm.

https://doi.org/10.1021/acsomega.4c07724
ACS Omega 2024, 9, 42582−42592

Furthermore, the overexpression of Smad 3 is closely associated with tissue fibrosis, where its overactivation can lead to increased collagen deposition, prompting excessive accumulation of the extracellular matrix and ultimately triggering tissue fibrosis.[36] In contrast, Smad 6 primarily functions as a negative regulator of TGF-β signaling, which can hinder the phosphorylation of Smad 3 and thereby slow down the process of tissue fibrosis.[37] As shown in Figure 5B, the prostate tissues of rats in the model group exhibited obvious green fluorescence (Smad 3), while red fluorescence (Smad 6) was nearly absent, indicating a notable fibrotic phenomenon. However, the high dose group exhibited the opposite scenario, with a significant increase in Smad 6 expression and almost no expression of Smad 3, suggesting the effective inhibition of prostate tissue fibrosis by Lut−Cu@HA.

4. CONCLUSIONS

In this study, a Lut−Cu@HA nanodelivery system was prepared, and it was demonstrated by physical characterization, in vitro performance testing, and in vivo efficacy evaluation that the nanoparticle has good water solubility, high safety, and a therapeutic effect on bacterial prostatitis in rats. This suggests that the nanoparticle has great potential in the clinical treatment of bacterial prostatitis. This not only provides a new idea for the treatment of bacterial prostatitis but also lays a theoretical and practical foundation for the wide application of luteolin in clinical practice.

■ ASSOCIATED CONTENT

Supporting Information

The Supporting Information is available free of charge at https://pubs.acs.org/doi/10.1021/acsomega.4c07724.

The absorption curve of Lut−Cu; the standard curve of Lut−Cu; the zeta potential variation of Lut−Cu@HA in aqueous solution (PDF)

■ AUTHOR INFORMATION

Corresponding Authors

Ke Wang − *School of Pharmacy, Health Science Center, Xi'an Jiaotong University, Xi'an, Shaanxi Province 710061, China*; orcid.org/0000-0002-6576-3370; Email: perpetual1003@mail.xjtu.edu.cn

Yanyao Gao − *Department of Urology, Tangdu Hospital, Air Force Medical University, Xi'an 710038, China*; Email: BigGemini8869@163.com

Jianxin Ni − *Urology and Nephrology Hospital, Xi'an People's Hospital (Xi'an Fourth Hospital), Xi'an, Shaanxi Province 710199, China*; Email: nijianxin@tom.com

Authors

Ruixiao Li − *Urology and Nephrology Hospital, Xi'an People's Hospital (Xi'an Fourth Hospital), Xi'an, Shaanxi Province 710199, China*

Yunhe Zheng − *School of Pharmacy, Health Science Center, Xi'an Jiaotong University, Xi'an, Shaanxi Province 710061, China*; orcid.org/0009-0002-5620-5470

Xuelian Li − *Department of Surgery, Xi'an Hospital of Traditional Chinese Medicine, Xi'an, Shaanxi Province 710000, China*

Ruiping Su − *Urology and Nephrology Hospital, Xi'an People's Hospital (Xi'an Fourth Hospital), Xi'an, Shaanxi Province 710199, China*

Jiangchuan He − *School of Pharmacy, Health Science Center, Xi'an Jiaotong University, Xi'an, Shaanxi Province 710061, China*; orcid.org/0009-0000-2002-6708

Song Xue − *Urology and Nephrology Hospital, Xi'an People's Hospital (Xi'an Fourth Hospital), Xi'an, Shaanxi Province 710199, China*

Complete contact information is available at: https://pubs.acs.org/10.1021/acsomega.4c07724

Author Contributions

#R.L. and Y.Z. contributed equally to this work.

Notes

The authors declare no competing financial interest.

■ ACKNOWLEDGMENTS

This study is financially supported by the National Natural Science Foundation of China (grant no. 32171336) and the Open Research Fund of Yunnan Characteristic Plant Extraction Laboratory (YKKF2023004). The Open Funds for Shaanxi Provincial Key Laboratory of Infection and Immune Diseases (2023-KFZD-1). The Open Projects Fund of Shandong Key Laboratory of Carbohydrate Chemistry and Glycobiology, Shandong University (no. 2023CCG02).

■ REFERENCES

(1) Liu, C.-P.; Chen, Z.-D.; Ye, Z.-Y.; He, D.-Y.; Dang, Y.; Li, Z.-W.; Wang, L.; Ren, M.; Fan, Z.-J.; Liu, H.-X. Therapeutic Applications of Functional Nanomaterials for Prostatitis. *Front. Pharmacol.* **2021**, *12*, 685465.

(2) Marquez-Algaba, E.; Burgos, J.; Almirante, B. Pharmacotherapeutic interventions for the treatment of bacterial prostatitis. *Expert Opin. Pharmacother.* **2022**, *23* (9), 1091−1101.

(3) Burgos, J.; Hoyos-Mallecot, Y.; Ferre-Losa, C.; Arando, M.; Monforte, A.; Pumarola, T.; Los-Arcos, I.; Falcó, V. Oral fosfomycin for treatment of acute bacterial prostatitis caused by multidrug-resistant Enterobacterales. *Microbiol. Spectrum* **2023**, *11* (5), No. e02136-23.

(4) Diedrich, C.; Zittlau, I. C.; Khalil, N. M.; Leontowich, A. F. G.; Freitas, R. A. D.; Badea, I.; Mainardes, R. M. Optimized Chitosan-Based Nanoemulsion Improves Luteolin Release. *Pharmaceutics* **2023**, *15* (6), 1592.

(5) Chen, L.; Chang, S.; Zhao, L.; Li, B.; Zhang, S.; Yun, C.; Wu, X.; Meng, J.; Li, G.; Guo, S. Biosynthesis of a water solubility-enhanced succinyl glucoside derivative of luteolin and its neuroprotective effect. *Microb. Biotechnol.* **2022**, *15* (9), 2401−2410.

(6) (a) Mutalik, C.; Lin, I.-H.; Krisnawati, D. I.; Khaerunnisa, S.; Khafid, M.; Widodo; Hsiao, Y.-C.; Kuo, T.-R. Antibacterial Pathways in Transition Metal-Based Nanocomposites: A Mechanistic Overview. *Int. J. Nanomed.* **2022**, *17*, 6821−6842. (b) Jomova, K.; Hudecova, L.; Lauro, P.; Simunková, M.; Barbierikova, Z.; Malcek, M.; Alwasel, S. H.; Alhazza, I. M.; Rhodes, C. J.; Valko, M. The effect of Luteolin on DNA damage mediated by a copper catalyzed Fenton reaction. *J. Inorg. Biochem.* **2022**, *226* (226), 111635. (c) Manman, H.; Weilan, C.; Zhimin, L.; Liang, P.; Lixia, H.; Min, C. ESI-TOF MS analysis of complexes formed between quercetin and five metal ions in hot water and a study into their DNA cleavage activity. *J. Inorg. Biochem.* **2019**, *195* (195), 13−19. (d) Roy, S.; Chakraborty, T. Deciphering the molecular mechanism and apoptosis underlying the in-vitro and in-vivo chemotherapeutic efficacy of vanadium luteolin complex in colon cancer. *Cell Biochem. Funct.* **2018**, *36* (3), 116−128. (e) Song, M.-T.; Wang, W.-Z.; Lu, Y.; Han, R.-M.; Skibsted, L. H.; Zhang, J.-P. Double-Site Binding and Anti-/Pro-oxidation of Luteolin on Bovine Serum Albumin Mediated by Copper(II) Coordination. *ACS Omega* **2022**, *7* (23), 19521−19534. (f) Xu, Y.; Yang, J.; Lu, Y.; Qian, L.-L.; Yang, Z.-Y.; Han, R.-M.; Zhang, J.-P.; Skibsted, L. H. Copper(II)

Coordination and Translocation in Luteolin and Effect on Radical Scavenging. *J. Phys. Chem. B* **2020**, *124* (2), 380−388.
(7) Malacaria, L.; La Torre, C.; Furia, E.; Fazio, A.; Caroleo, M. C.; Cione, E.; Gallelli, L.; Marino, T.; Plastina, P. Aluminumiron(III), (III) and copper(II) complexes of luteolin: Stability, antioxidant, and anti-inflammatory properties. *J. Mol. Liq.* **2022**, *345*, 117895.
(8) Gao, Y.; Liu, K.; Zhang, Y.; Sun, Z.; Song, B.; Wang, Y.; Zhang, B.; Chen, X.; Hu, D.; Wen, J. Hyaluronic acid-modified curcumin-copper complex nano delivery system for rapid healing of bacterial prostatitis. *Carbohydr. Polym.* **2023**, *310*, 120668.
(9) Cheng, Q.; Liu, C.; Zhao, J.; Li, W.; Guo, F.; Qin, J.; Wang, Y. Unlocking the potential of hyaluronic acid: Exploring its physicochemical properties, modification, and role in food applications. *Trends Food Sci. Technol.* **2023**, *142*, 104218.
(10) Yasin, A.; Ren, Y.; Li, J.; Sheng, Y.; Cao, C.; Zhang, K. Advances in Hyaluronic Acid for Biomedical Applications. *Front. Bioeng. Biotechnol.* **2022**, *10*, 910290.
(11) Neves, M. I.; Araújo, M.; Moroni, L.; da Silva, R. M. P.; Barrias, C. C. Glycosaminoglycan-Inspired Biomaterials for the Development of Bioactive Hydrogel Networks. *Molecules* **2020**, *25* (4), 978.
(12) Katoh, S.; Maeda, S.; Fukuoka, H.; Wada, T.; Moriya, S.; Mori, A.; Yamaguchi, K.; Senda, S.; Miyagi, T. A crucial role of sialidase Neu1 in hyaluronan receptor function of CD44 in T helper type 2-mediated airway inflammation of murine acute asthmatic model. *Clin. Exp. Immunol.* **2010**, *161* (2), 233−241.
(13) Sanidad, K. Z.; Sukamtoh, E.; Xiao, H.; McClements, D. J.; Zhang, G. Curcumin: Recent Advances in the Development of Strategies to Improve Oral Bioavailability. *Annu. Rev. Food Sci. Technol.* **2019**, *10* (1), 597−617.
(14) Shimoi, K.; Okada, H.; Furugori, M.; Goda, T.; Takase, S.; Suzuki, M.; Hara, Y.; Yamamoto, H.; Kinae, N. Intestinal absorption of luteolin and luteolin 7-O-β-glucoside in rats and humans. *FEBS Lett.* **1998**, *438* (3), 220−224.
(15) Chen, C.-Y.; Peng, W.-H.; Tsai, K.-D.; Hsu, S.-L. Luteolin suppresses inflammation-associated gene expression by blocking NF-κB and AP-1 activation pathway in mouse alveolar macrophages. *Life Sci.* **2007**, *81* (23), 1602−1614.
(16) Sakurai, M. A.; Ozaki, Y.; Okuzaki, D.; Naito, Y.; Sasakura, T.; Okamoto, A.; Tabara, H.; Inoue, T.; Hagiyama, M.; Ito, A. Gefitinib and Luteolin Cause Growth Arrest of Human Prostate Cancer PC-3 Cells via Inhibition of Cyclin G-Associated Kinase and Induction of miR-630. *PLoS One* **2014**, *9* (6), No. e100124.
(17) Ntalouka, F.; Tsirivakou, A. Luteolin: A promising natural agent in management of pain in chronic conditions. *Front Pain Res.* **2023**, *4*, 1114428.
(18) Roy, S.; Mallick, S.; Chakraborty, T.; Ghosh, N.; Singh, A. K.; Manna, S.; Majumdar, S. Synthesis, characterisation and antioxidant activity of luteolin-vanadium(II) complex. *Food Chem.* **2015**, *173*, 1172−1178.
(19) Li, Y.; Chen, X.; Zhou, Z.; Fang, B.; Chen, Z.; Huang, Y.; Hu, Y.; Liu, H. Berberine oleanolic acid complex salt grafted hyaluronic acid/silk fibroin (BOA-g-HA/SF) composite scaffold promotes cartilage tissue regeneration under IL-1β caused stress. *Int. J. Biol. Macromol.* **2023**, *250*, 126104.
(20) Hu, D.; Wen, J.; Zhao, X.; Liu, K.; Zhang, Y.; Bu, Y.; Wang, K. A wound-friendly antibacterial hyaluronic acid dressing with on-demand removability for infected wound healing. *Biomater. Res.* **2023**, *27* (1), 38.
(21) Nagano, K.; Nakao, T.; Takeda, M.; Hirai, H.; Maekita, H.; Nakamura, M.; Imakawa, N.; Egawa, A.; Fujiwara, T.; Gao, J.-Q.; et al. Polyglycerol fatty acid ester contributes to the improvement and maintenance of water solubility of amorphous curcumin by suppressing the intermolecular interaction and the diffusion rate of curcumin. *Food Chem.* **2024**, *437*, 137866.
(22) Su, R.; Su, W.; Cai, J.; Cen, L.; Huang, S.; Wang, Y.; Li, P. Photodynamic antibacterial application of TiO2/curcumin/hydroxypropyl-cyclodextrin and its konjac glucomannan composite films. *Int. J. Biol. Macromol.* **2024**, *254*, 127716.
(23) Shah, V. P.; Simona Miron, D.; Ştefan Rădulescu, F.; Cardot, J.-M.; Maibach, H. I. In vitro release test (IVRT): Principles and applications. *Int. J. Pharm.* **2022**, *626*, 122159.
(24) de la Fuente-Jiménez, J. L.; Rodríguez-Rivas, C. I.; Mitre-Aguilar, I. B.; Torres-Copado, A.; García-López, E. A.; Herrera-Celis, J.; Arvizu-Espinosa, M. G.; Garza-Navarro, M. A.; Arriaga, L. G.; García, J. L.; et al. A Comparative and Critical Analysis for In Vitro Cytotoxic Evaluation of Magneto-Crystalline Zinc Ferrite Nanoparticles Using MTT, Crystal Violet, LDH, and Apoptosis Assay. *Int. J. Mol. Sci.* **2023**, *24* (16), 12860.
(25) (a) Inci, M.; Davarci, M.; Inci, M.; Motor, S.; Yalcinkaya, F. R.; Nacar, E.; Aydin, M.; Sefil, N. K.; Zararsız, I. Anti-inflammatory and antioxidant activity of thymoquinone in a rat model of acute bacterial prostatitis. *Hum. Exp. Toxicol.* **2013**, *32* (4), 354−361. (b) Zheng, J.; Hu, R.; Yang, Y.; Wang, Y.; Wang, Q.; Xu, S.; Yao, P.; Liu, Z.; Zhou, J.; Yang, J. Antibiotic-loaded reactive oxygen species-responsive nanomedicine for effective management of chronic bacterial prostatitis. *Acta Biomater.* **2022**, *143* (143), 471−486.
(26) (a) Wang, L.; Hou, Y.; Wang, R.; Pan, Q.; Li, D.; Yan, H.; Sun, Z. Inhibitory Effect of Astaxanthin on Testosterone-Induced Benign Prostatic. *Hyperplasia In Rats. Marine Drugs* **2021**, *19* (12), 652. (b) Huang, Q.; Wang, J.; Zong, R.; Wu, D.; Jin, C. A Water-Soluble Polysaccharide from the Fibrous Root of Anemarrhena asphodeloides Bge. and Its Immune Enhancement Effect in Vivo and in Vitro. *Evidence-Based Complementary Altern. Med.* **2022**, *2022*, 8723119. (c) Wu, F.; Ding, X.-Y.; Li, X.-H.; Gong, M.-J.; An, J.-Q.; Huang, S.-L. Correlation between elevated inflammatory cytokines of spleen and spleen index in acute spinal cord injury. *J. Neuroimmunol.* **2020**, *344* (344), 577264.
(27) Zhao, X.; Wang, L.; Gao, J.; Chen, X.; Wang, K. Hyaluronic acid/lysozyme self-assembled coacervate to promote cutaneous wound healing. *Biomater. Sci.* **2020**, *8* (6), 1702−1710.
(28) Gao, J.; Wen, J.; Hu, D.; Liu, K.; Zhang, Y.; Zhao, X.; Wang, K. Bottlebrush inspired injectable hydrogel for rapid prevention of postoperative and recurrent adhesion. *Bioact. Mater.* **2022**, *16*, 27−46.
(29) Sæbø, I.; Bjørås, M.; Franzyk, H.; Helgesen, E.; Booth, J. Optimization of the Hemolysis Assay for the Assessment of Cytotoxicity. *Int. J. Mol. Sci.* **2023**, *24* (3), 2914.
(30) Lv, F.; Zhang, Y.; Peng, Q.; Zhao, X.; Hu, D.; Wen, J.; Liu, K.; Li, R.; Wang, K.; Sun, J. Apigenin-Mn(II) loaded hyaluronic acid nanoparticles for ulcerative colitis therapy in mice. *Front. Chem.* **2022**, *10*, 969962.
(31) Niu, S.; Han, B.; Cao, W.; Zhang, S. Sensitive DNA biosensor improved by Luteolin copper(II) as indicator based on silver nanoparticles and carbon nanotubes modified electrode. *Anal. Chim. Acta* **2009**, *651* (1), 42−47.
(32) Anitha, A.; Deepagan, V. G.; Divya Rani, V. V.; Menon, D.; Nair, S. V.; Jayakumar, R. Preparation, characterization, in vitro drug release and biological studies of curcumin loaded dextran sulphate−chitosan nanoparticles. *Carbohydr. Polym.* **2011**, *84* (3), 1158−1164.
(33) Wanninger, S.; Lorenz, V.; Subhan, A.; Edelmann, F. T. Metal complexes of curcumin–synthetic strategies, structures and medicinal applications. *Chem. Soc. Rev.* **2015**, *44* (15), 4986−5002.
(34) Chae, B. J.; Lee, K.-S.; Hwang, I.; Yu, J.-W. Extracellular Acidification Augments NLRP3-Mediated Inflammasome Signaling in Macrophages. *Immune Network* **2023**, *23* (3), No. e23.
(35) Brierly, G.; Celentano, A.; Breik, O.; Moslemivayeghan, E.; Patini, R.; McCullough, M.; Yap, T. Tumour Necrosis Factor Alpha (TNF-α) and Oral Squamous Cell Carcinoma. *Cancers* **2023**, *15* (6), 1841.
(36) Flanders, K. C. Smad3 as a mediator of the fibrotic response. *Int. J. Exp. Pathol.* **2004**, *85* (2), 47−64.
(37) Park, S.-H. Fine Tuning and Cross-talking of TGF-β Signal by Inhibitory Smads. *BMB Rep.* **2005**, *38* (1), 9−16.

https://doi.org/10.1021/acsomega.4c07724
ACS Omega 2024, 9, 42582−42592